THE LANCET
Planetary Health

Supplementary appendix

This appendix formed part of the original submission and has been peer reviewed. We post it as supplied by the authors.

Supplement to: Giani P, Castruccio S, Anav A, Howard D, Hu W, Crippa P. Short-term and long-term health impacts of air pollution reductions from COVID-19 lockdowns in China and Europe: a modelling study. *Lancet Planet Health* 2020; published online Sept 22. http://dx.doi.org/10.1016/S2542-5196(20)30224-2.

Appendix to manuscript

Short- and long-term health impacts of air pollution reductions from COVID-19 lockdowns in China and Europe

Paolo Giani[1], Stefano Castruccio[2], Alessandro Anav[3], Don Howard[4], Wenjing Hu[2], Paola Crippa[1*]

[1]Department of Civil and Environmental Engineering and Earth Sciences, University of Notre Dame, Notre Dame, IN, USA
[2]Department of Applied and Computational Mathematics and Statistics, University of Notre Dame, Notre Dame, IN, USA
[3]Climate Modeling Laboratory, ENEA, Italian National Agency for New Technologies, Energy and Sustainable Economic Development, CR Casaccia, Santa Maria di Galeria, Italy

[4]Department of Philosophy, University of Notre Dame, Notre Dame, IN, USA

*Corresponding author: Paola Crippa, Department of Civil and Environmental Engineering and Earth Sciences, University of Notre Dame, Notre Dame, IN 46556, USA, email: pcrippa@nd.edu

EVIDENCE OF IMPROVED AIR QUALITY

The air quality index (AQI) for both China and Europe showed an overall improvement during the first quarter of 2020 as a response to the wide range of interventions implemented by national governments to contain the spread of COVID-19. In China, during the first 30 days following the shutdown (January 29 to February 29), 46% of the monitoring stations indicated a good to excellent air quality (AQI<=50) against 34% in the same period in 2019. For heavily to severely polluted air quality (AQI>100) during the same days, in 2020 only 2% of the stations indicated it against 7% in 2019. In some main cities in Europe, ground observations in the week of 16th-22th March highlighted a sharp decrease, between 20% and 60%, of nitrogen dioxide (NO_2) concentrations against the same week in 2019[1,2]. Similar conclusions can be drawn from satellite observations[3] which show a significant decrease in NO_2 concentrations in February and March as a result of the lockdown of most of the anthropogenic activities (Figure S1).

We analyze the differences between $PM_{2.5}$ concentrations during post-outbreak period and the same period from several previous years (2016-2019), to gain insights on the drivers of the air quality changes observed after COVID-19 outbreak. Even though interannual meteorological fluctuations can considerably affect $PM_{2.5}$ concentrations[4,5], the observed decrease in $PM_{2.5}$ throughout China cannot be ascribed to meteorological variations alone (Figure S2, Table S4 and Table S7). The population-weighted mean $PM_{2.5}$ during February-March 2020 is statistically lower than the natural meteorological variability, as suggested by the p-values obtained by pairing 2020 concentrations with the same period in previous years (<<0.001, Table S7). This pattern is even more evident for Hubei province and other provinces highly impacted by lockdown measures (e.g. Zhejiang, Guangxi, Shaanxi, Henan, Shandong, Table S4). In Europe, the meteorological fluctuations play a more significant role in influencing 2020 concentrations. Although population-weighted mean $PM_{2.5}$ during the lockdown period (21 February-17 May) is also considerably lower than 2016-2019, the statistical significance is weaker (Table S6). Exceptionally low $PM_{2.5}$ concentrations have been observed during the second half of February and the beginning of March, whereas $PM_{2.5}$ accumulated in most of central Europe toward the end of March (Figure S3) because of westward transport from Eastern Europe and unfavorable meteorological conditions that suppressed the dispersion of pollutants (i.e., a high-pressure system was in place during March 21-March 28, Figure S4).

METHODS

$PM_{2.5}$ OBSERVATIONS

Hourly $PM_{2.5}$ observations for Mainland China, Hong Kong and Europe are retrieved from online archives of the Ministry of Ecology and Environment (http://beijingair.sinaapp.com/), the Hong Kong Environmental Protection Department (https://www.epd.gov.hk/epd) and the European Environment Agency (http://www.eionet.europa.eu/aqportal), for 2016-2020. In our analysis, we only focus on European countries with at least one air quality station that reported $PM_{2.5}$ data for 2020 on June 30. The list of European countries included in our analysis is reported in Table S2. As of 2020, the Chinese network comprises more than 1,600 stations with valid data in the considered timeframe, while the European sites that to date have reported their data are approximately 1,000. $PM_{2.5}$ daily means are computed at each site after preprocessing steps to ensure data quality. Specifically we remove negative zero values, consecutive repeats of hourly $PM_{2.5}$ concentrations for 4 or more hours, and daily average when more than 30% of the hourly data in a day are zero/missing. For European data, we only consider data flagged as "valid" or "valid but below detection limit" in the database.

$PM_{2.5}$ DAILY FIELD ESTIMATION

Our analysis combines different data sources to accurately estimate daily $PM_{2.5}$ concentration fields in previous years (2016-2019) and during the COVID-19 outbreak (2020). We employ a widely used Gaussian process regression interpolation technique (i.e., ordinary kriging[6]), with a deterministic mean trend surface modeled via a first order polynomial with WRF-Chem output as the only covariate:

$$z(s) = \mu(s) + \varepsilon(s), \quad (1)$$

$$\mu(s) = \beta_0 + \beta_1 x(s). \quad (2)$$

In Equation (1), $z(s)$ is the target $PM_{2.5}$ concentration field, s is the spatial coordinate (two-dimensional), $\mu(s)$ is the deterministic mean trend surface, $x(s)$ is the $PM_{2.5}$ concentration given by the numerical model simulation and $\varepsilon(s)$ is a Gaussian field with a spherical covariance function[6]. The mean surface concentration is thus estimated by correcting the numerical model simulation with available observations and $\varepsilon(s)$ is estimated via interpolation and added to the mean surface concentration with a kriging procedure. All the parameters in the model (β_0, β_1 and the covariance function of $\varepsilon(s)$) are estimated on a daily basis to obtain daily $PM_{2.5}$ concentration fields. This being a stochastic model (i.e., $\varepsilon(s)$ is a random field), we can efficiently obtain new random realizations of the process that preserve the main statistics of the estimated field for uncertainty quantification purposes[7]. All calculations are performed in log-space to avoid unphysical negative $PM_{2.5}$ concentrations and to account for the inherent log-normality of observed $PM_{2.5}$ observed data.

The methodology described here has been applied and validated previously in the literature and showed good skills in reproducing $PM_{2.5}$ concentrations with cross-validation procedures[8]. For the present study, we report similar cross-validation results for the first semester of 2019/2020 (Figure S6 and S7). The model is able to capture $PM_{2.5}$ concentrations both in the typical range and during COVID-19 outbreak, as it is calibrated on observed data. Cross-validation mean bias is close to zero (-0.68 μg m^{-3} for European data and -1.11 μg m^{-3} for Chinese data), and the magnitude of Root Mean Square Error (RMSE) is less than 20% of the average $PM_{2.5}$ concentrations for both China and Europe (Figure S6 and S7). The performance metrics reported herein indicate similar bias and lower RMSE than analogous regional scale studies which make use of satellite observations (e.g. Bai et al., 2019; Xue et al., 2019).

EMISSION SCENARIOS OF FUTURE ECONOMIC RECOVERY

Here we provide details on the four pathways of future economic recovery adopted in this work and how they impact $PM_{2.5}$ concentrations.

1) Immediate resumption: this scenario assumes the lockdown interventions stop on April 1 in China and on May 17 in Europe, thus the annual $PM_{2.5}$ concentrations are lower than prior years as a result of the $PM_{2.5}$ decrease during the lockdown periods, whereas for the remainder of the year $PM_{2.5}$ levels return to their typical values (i.e., the average between 2016 and 2019). We consider a 4-year average as typical concentrations to smooth out the meteorological variability.

2) Gradual resumption: this scenario is an analog for either a reaction/management of a prolonged pandemic crisis or reduced emissions associated with technological advances and/or changes to working habits and lifestyles (e.g., more remote working, reduced per capita energy consumptions). It assumes a progressive recovery in human activities, and thus a proportional increase of $PM_{2.5}$ concentrations during April 1 – June 30 in China and during May 18 – August 18 in Europe. Each model grid cell is scaled by a coefficient calculated as the ratio of $PM_{2.5}$ concentrations during the post outbreak period and the same period during 2016-2019, on the first resumption day. The coefficients are then linearly increased every day until they reach 1 (i.e., typical concentrations) at the end of the three months recovery.

3) Fall outbreak: viral diseases are often characterized by seasonal outbreaks[9,10], although it is still debated whether coronavirus will be weaker/latent during the summer in the Northern Hemisphere[11]. This scenario accounts for the possibility of a second coronavirus outbreak in the fall, which will require again social distancing measures, analogously to the one experienced in the first semester of 2020. We assume that $PM_{2.5}$ concentrations sharply return to typical levels on April 1 in China and May 18 in Europe, and a second outbreak between October to December occurs, in which concentrations are scaled by the same reduction coefficients calculated during the first outbreak.

4) Permanent lockdown: in the absence of evidence of effective control strategies other than social distancing and no available vaccine or effective medical treatments able to contain the pandemic spread, the extreme scenario of a permanent lockdown for the whole of 2020 is considered. Typical $PM_{2.5}$ concentrations are thus decreased by the reduction coefficient calculated during the outbreak period for the remainder of the year.

ASSESSMENT OF THE UNCERTAINTY FOR THE MORTALITY ESTIMATES

Confidence intervals of mortality estimates are estimated via Monte Carlo simulations[8]. We propagate uncertainty in $PM_{2.5}$ fields, baseline mortality and RR parameters by sampling from the underlying probability distributions. The uncertainty in $PM_{2.5}$ fields is estimated through conditional simulations, i.e. random realizations of the Gaussian random field with mean and the covariance structure estimated with Equation (1) and Equation (2).

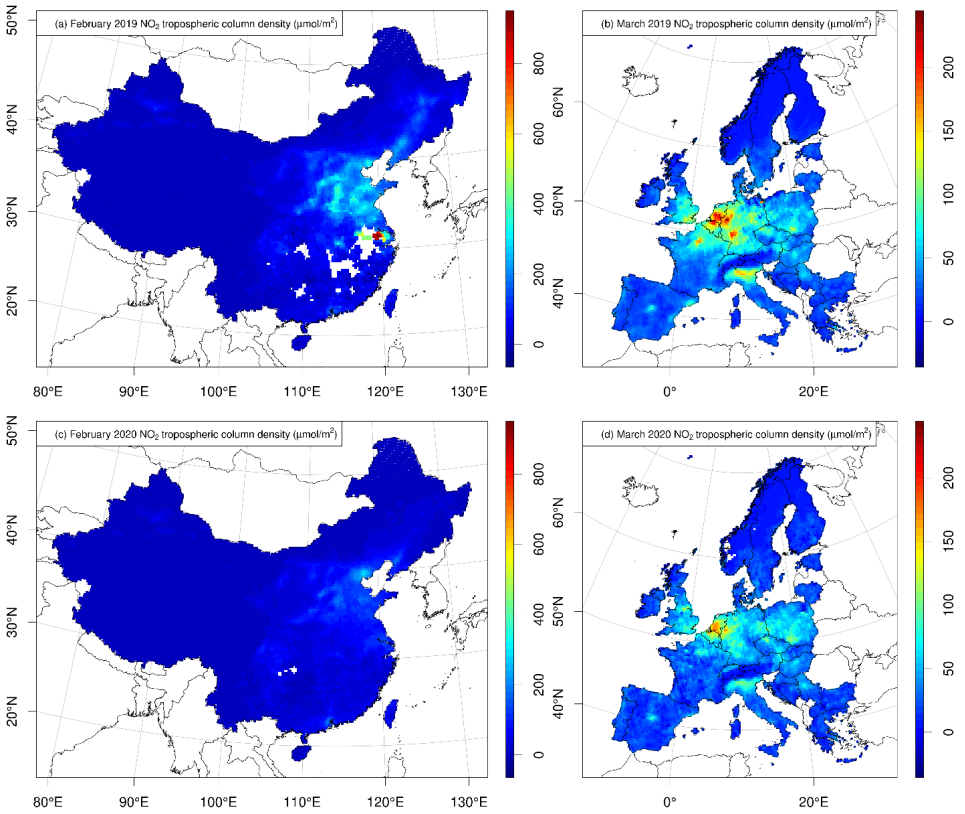

Figure S1. Effect of NO_2 emission reductions due to countries lockdown. Difference between monthly mean NO_2 tropospheric column density in 2020 and 2019 for (a-c) February in China and (b-d) March in Europe as detected by the NASA Ozone Monitoring Instrument.

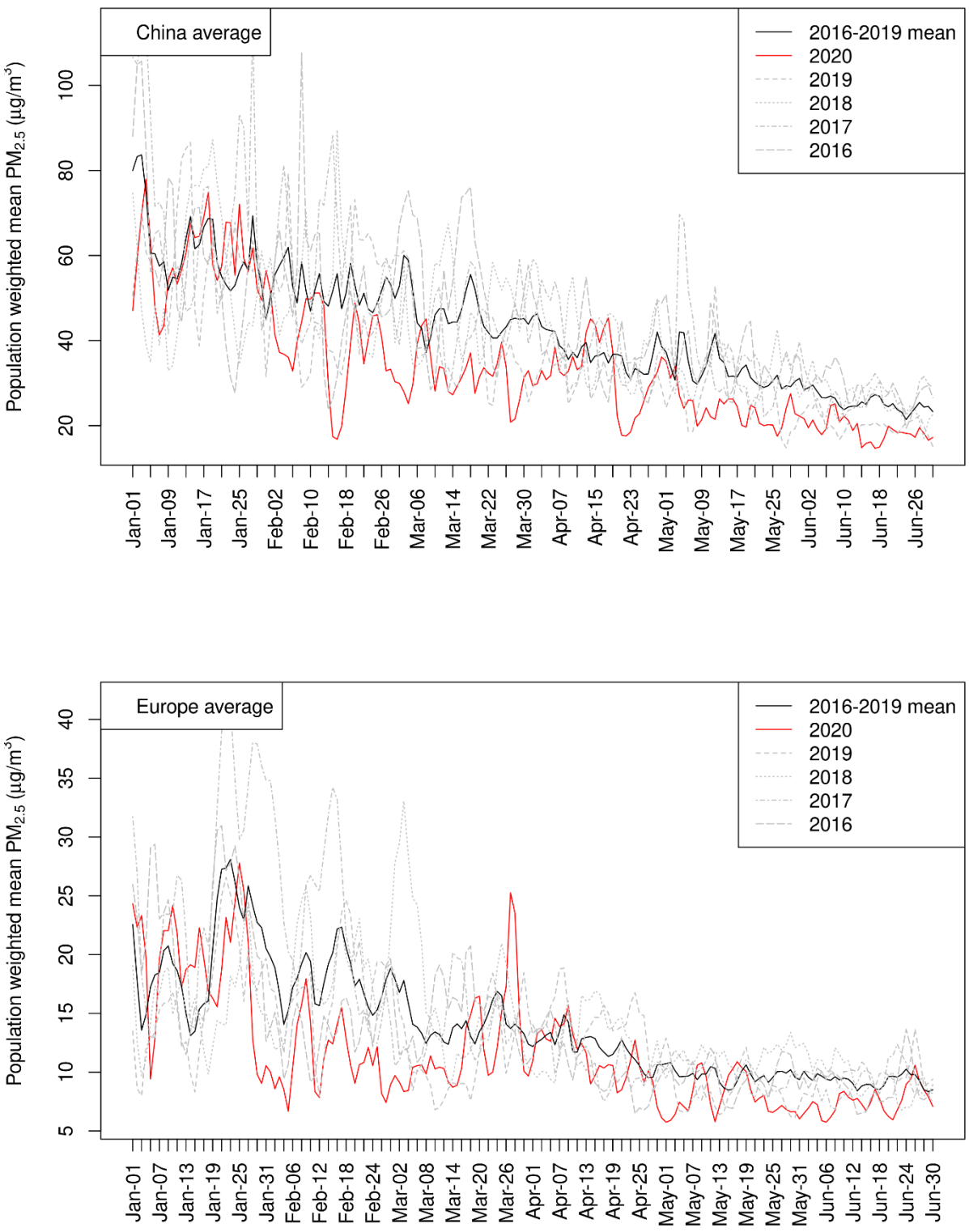

Figure S2. Comparison between population-weighted $PM_{2.5}$ timeseries between 2020 and previous years, for (top) China and (bottom) Europe.

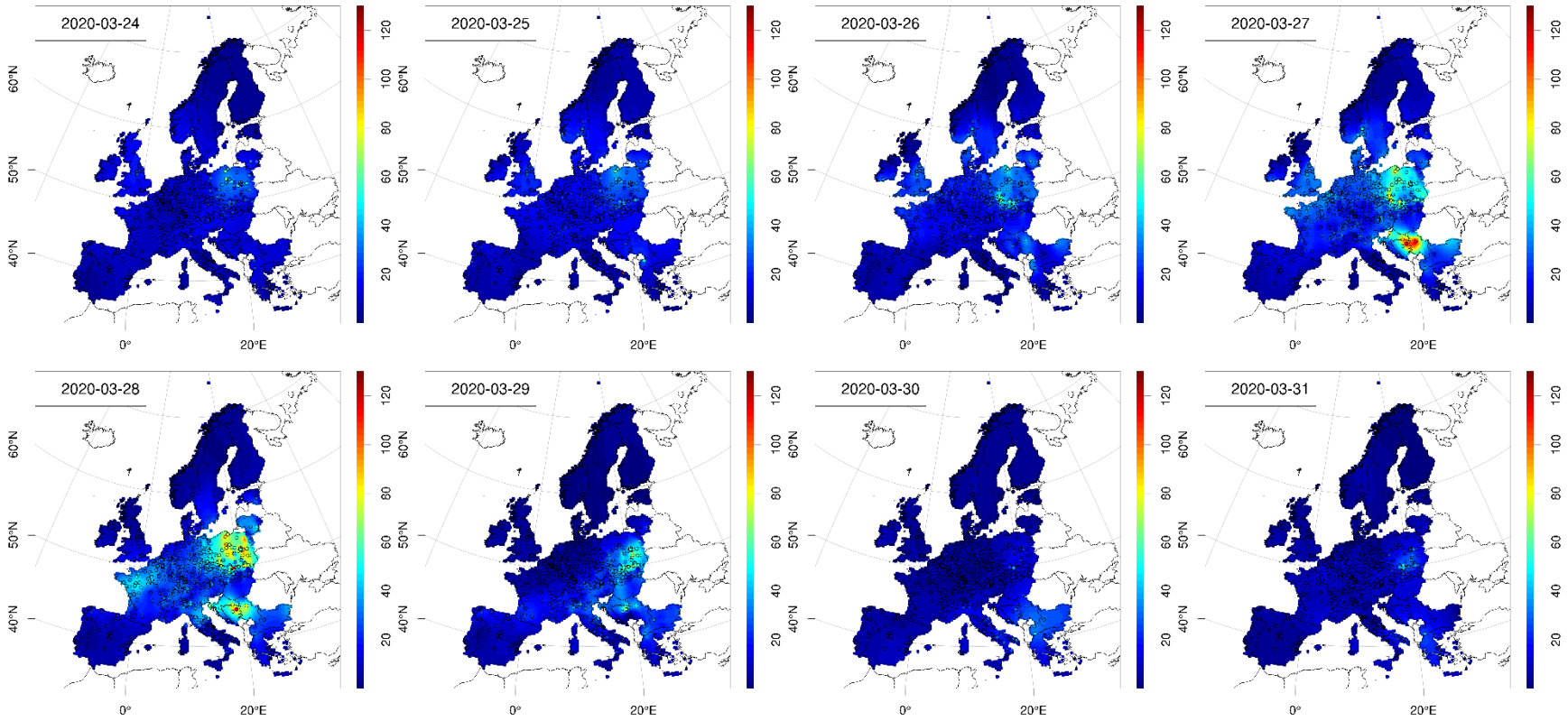

Figure S3. $PM_{2.5}$ daily fields during March 24 – 31 2020 in Europe.

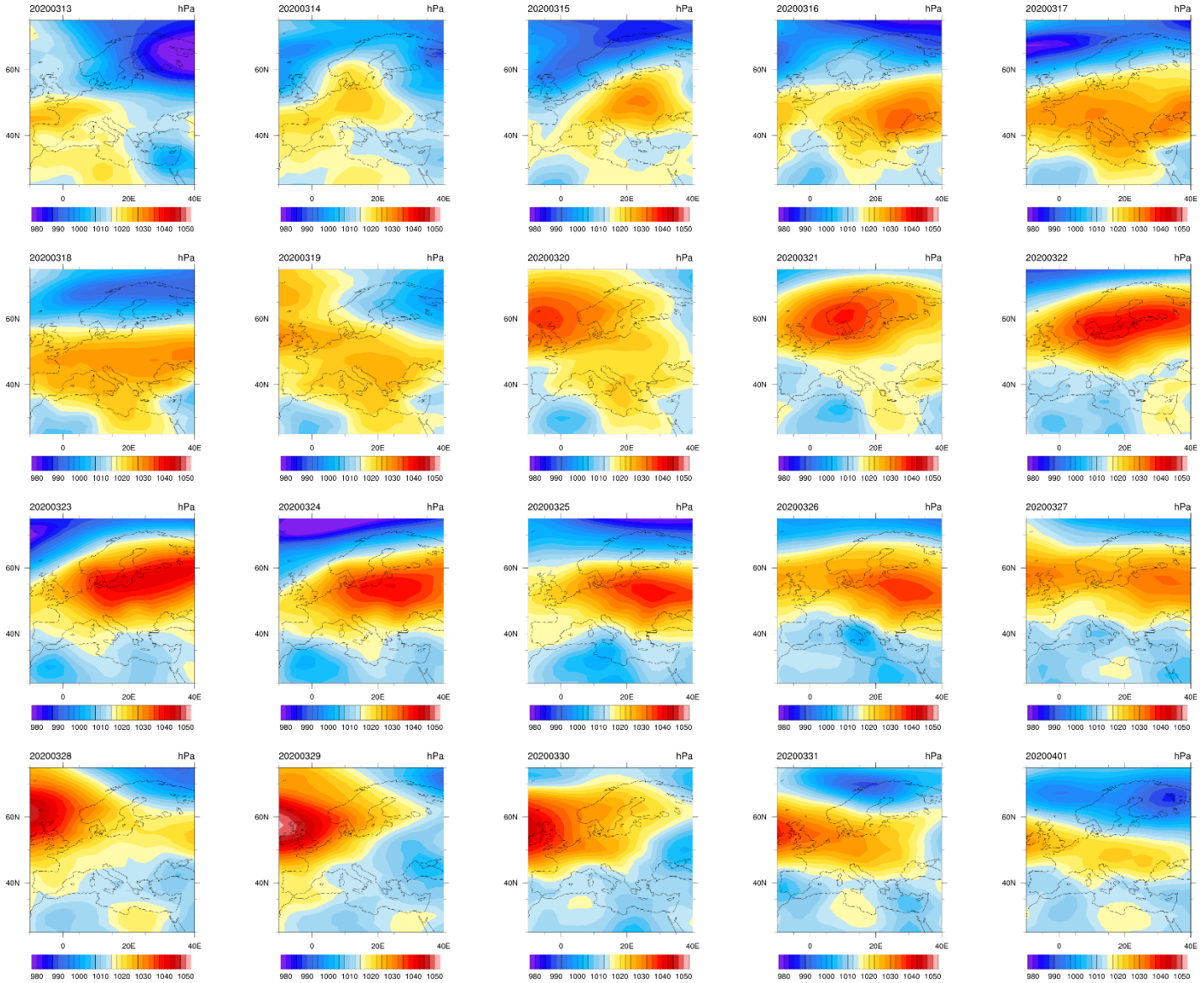

Figure S4. Sea-level pressure from NCEP/NCAR Reanalysis 1 for March 13 – 31 2020 in Europe.

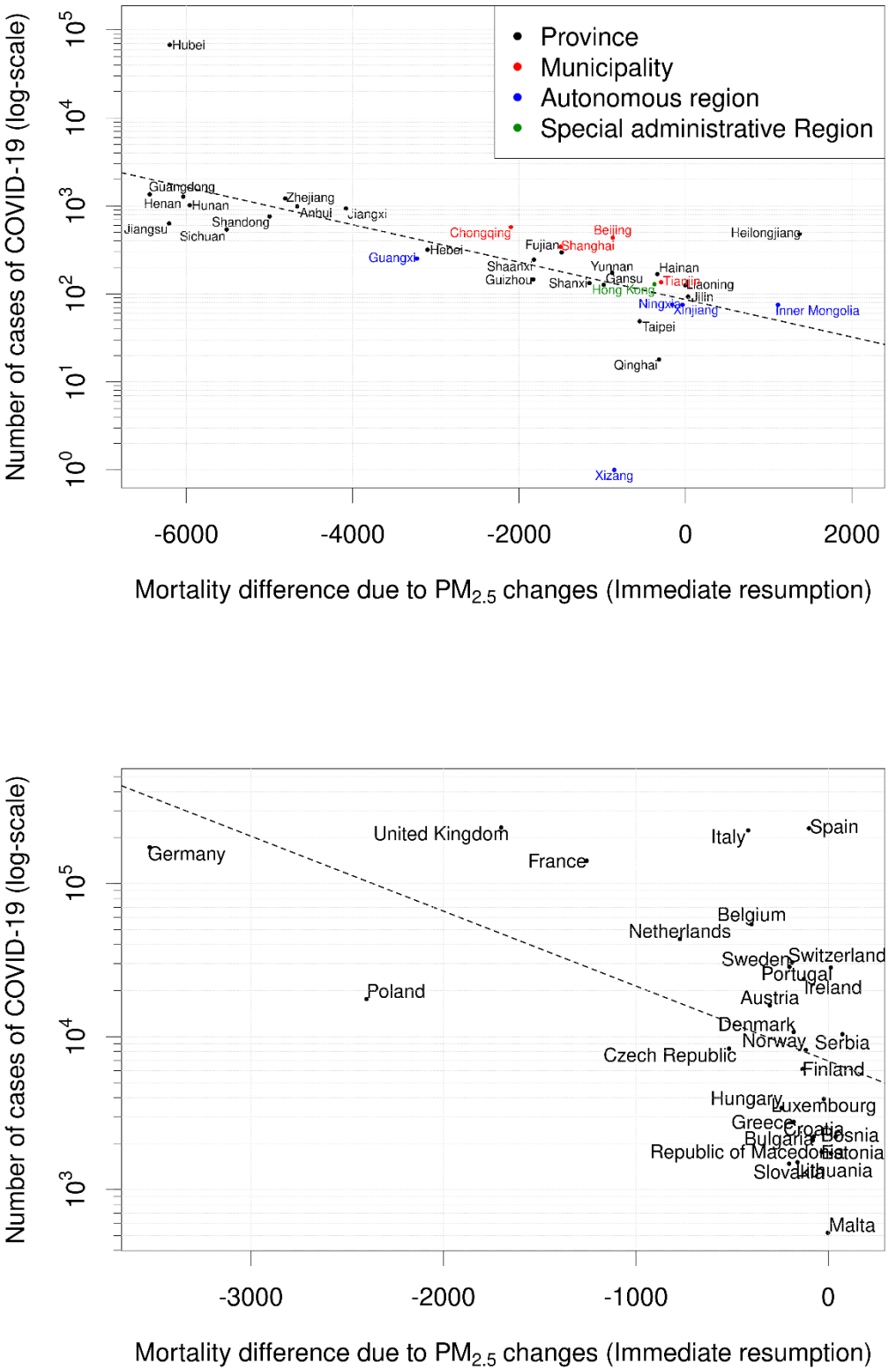

Figure S5. Number of COVID-19 cases for each province in China (top) and country in Europe (bottom), plotted against the long-term mortality difference due to $PM_{2.5}$ variations between 2020 and 2016-2019 average (Immediate Resumption scenario).

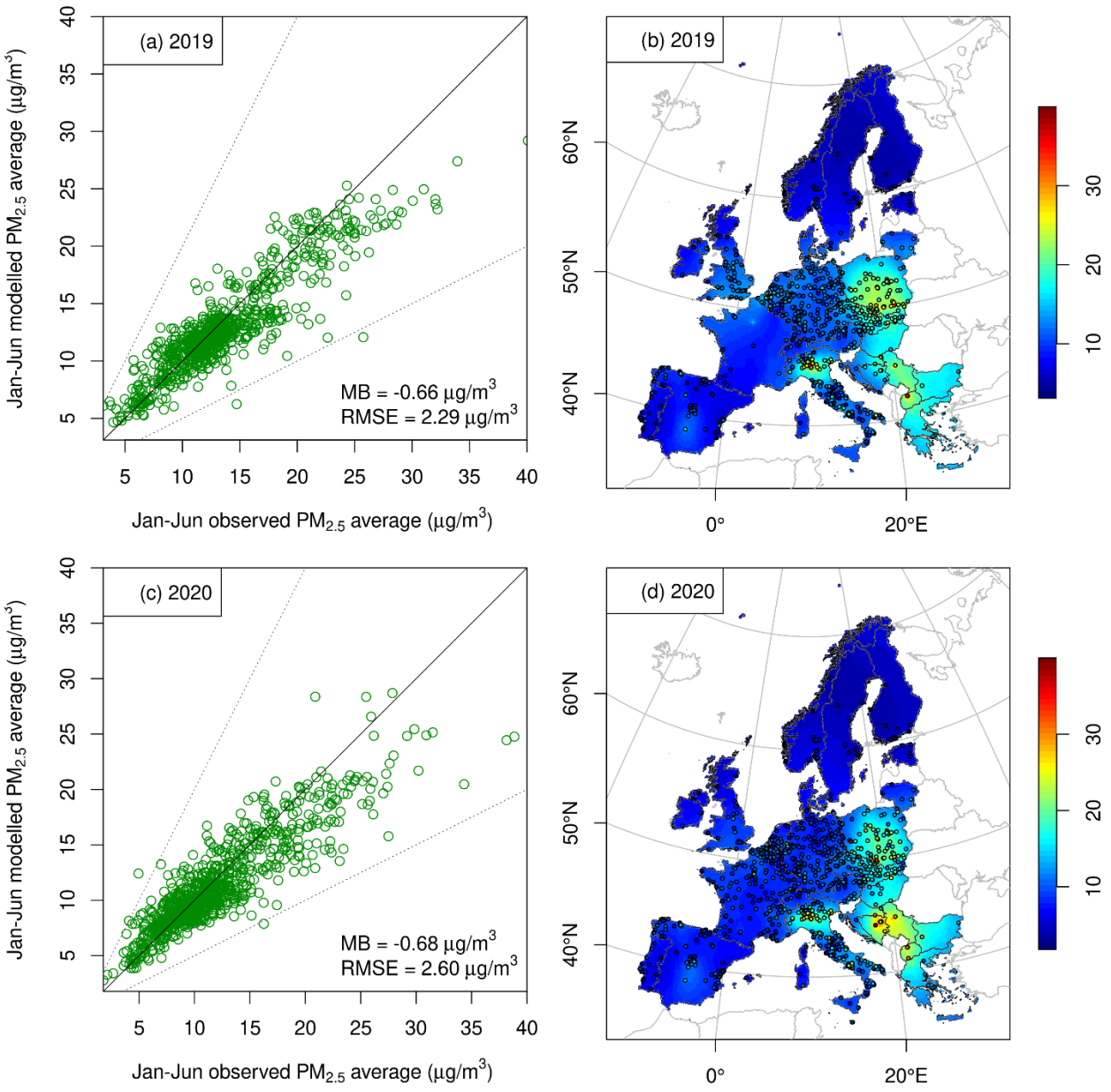

Figure S6. Cross-validation results $PM_{2.5}$ mean concentrations for the first semester of 2019 (top) and 2020 (bottom) in Europe. $PM_{2.5}$ concentration fields are reconstructed daily based on the methodology presented in the main text.

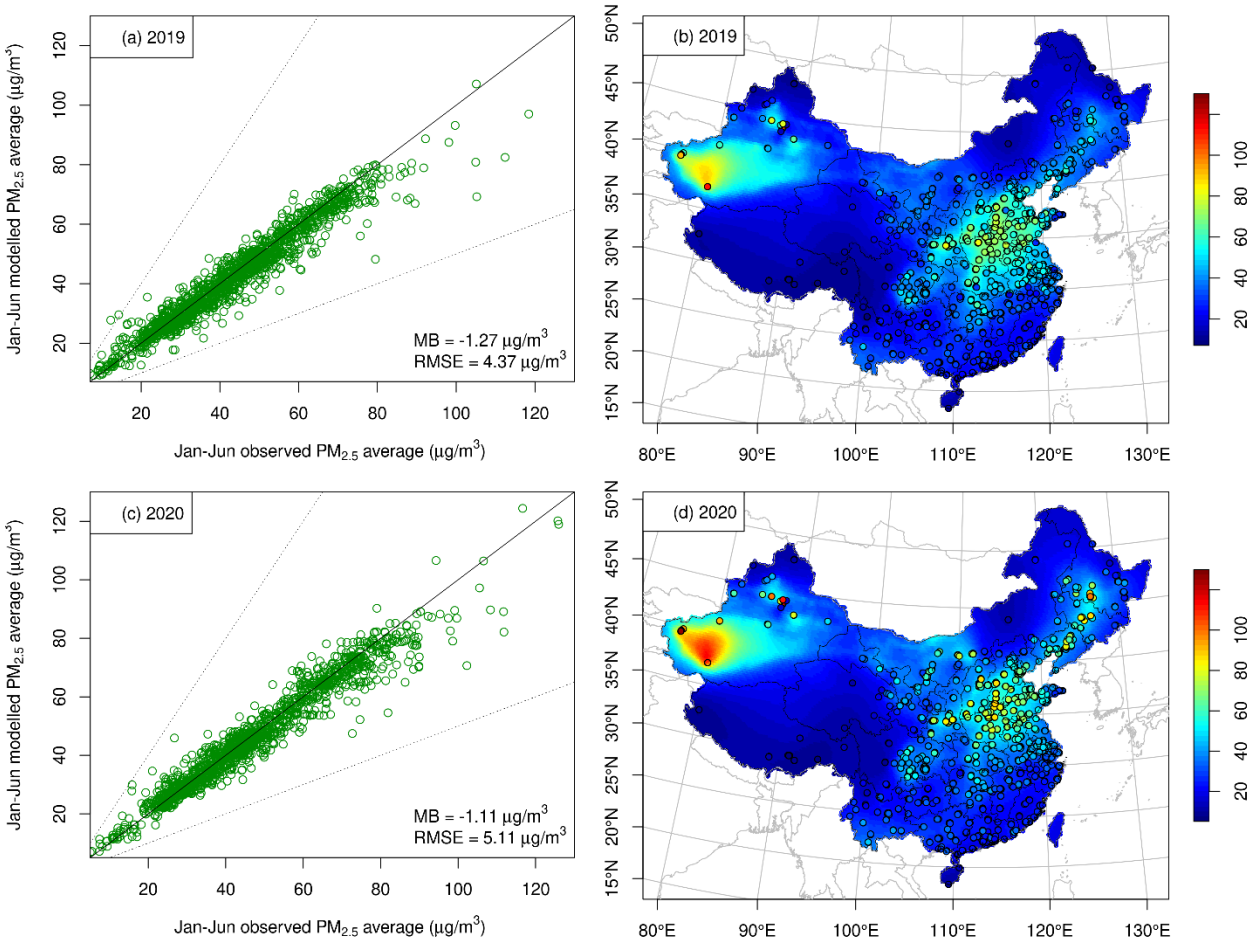

Figure S7. Cross-validation results $PM_{2.5}$ mean concentrations for the first semester of 2019 (top) and 2020 (bottom) in China. $PM_{2.5}$ concentration fields are reconstructed daily based on the methodology presented in the main text.

Table S1. Domain setup and physical and chemical schemes adopted for the WRF-Chem simulations presented in the work.

Domain	**Setup**
Size and grid cells	330 × 1441
Physics time step	20 seconds
Chemistry time step	5 minutes
Physics/Chemistry/Emission Option	**Adopted Scheme**
Microphysics	Single–moment 6–class [12]
Cumulus Parameterization	New Tiedtke [13]
Shortwave and Longwave Radiation	RRTMG [14]
Land-surface	Noah Land Surface Model [15]
Planetary boundary layer	Yonsei University Scheme [16]
Gas phase chemistry	MOZART [17]
Aerosol	GOCART [18]
Photolysis	Madronich F-TUV [19]
Biogenic emissions	MEGAN [20]
Anthropogenic emissions	EDGAR HTAP (v2.2) [21]
Fire emissions	FINN (v1.5) [22]
Dust emissions	GOCART [23]
Sea salt	Based on model in Gong [24]
Initial and Boundary conditions	Adopted Dataset
Meteorology	ERA5 [25], every 3 hours
Chemistry	MOZART-4/GEOS-5 [17], every 6 hours

Table S2. Population weighted average of $PM_{2.5}$ concentrations for all the European countries considered in this work, during the lockdown period (February 21 – May 17) over the years 2016-2020. Values in bold indicate that the difference between $PM_{2.5}$ concentrations in 2020 and the average of 2016-2019 are statistically significant at 1% significance level (with a paired t-test on daily averages).

Country	2016	2017	2018	2019	2016-2019 mean	2020
Austria	12.19	10.80	16.12	11.24	12.59	**10.04**
Belgium	12.83	12.42	15.67	14.00	13.73	**11.06**
Bosnia and Herzegovina	18.21	22.01	23.23	15.40	19.71	18.64
Bulgaria	15.40	15.25	15.85	15.37	15.47	14.90
Croatia	14.17	15.25	18.66	13.60	15.42	13.80
Czech Republic	15.83	13.83	21.29	14.99	16.48	**13.45**
Denmark	9.94	8.31	12.61	10.89	10.44	**7.26**
Estonia	7.35	5.50	8.42	6.01	6.82	**4.42**
Finland	5.98	4.07	5.83	5.77	5.41	**4.04**
France	12.07	10.41	11.55	11.14	11.29	**9.65**
Germany	12.33	10.63	15.13	11.83	12.48	**9.09**
Greece	15.60	15.85	15.73	16.55	15.93	**13.13**
Hungary	14.70	15.33	18.69	14.73	15.86	**13.97**
Ireland	8.95	7.62	9.15	12.01	9.43	**7.60**
Italy	13.38	14.66	13.92	13.32	13.82	13.11
Lithuania	14.45	13.40	17.37	11.52	14.18	**9.21**
Luxembourg	11.26	10.04	10.85	9.84	10.50	**8.36**
Malta	11.22	10.71	13.26	11.99	11.80	10.30
Netherlands	11.13	10.59	17.32	13.14	13.05	**9.25**
Norway	6.80	5.71	8.26	7.59	7.09	**5.46**
Poland	21.50	18.65	25.68	18.69	21.13	**17.49**
Portugal	6.20	8.11	7.91	7.63	7.46	7.04
Republic of Macedonia	14.59	19.72	14.69	21.05	17.51	18.63
Serbia	16.83	20.80	19.25	18.47	18.84	18.52
Slovakia	16.26	14.72	20.16	15.45	16.65	**14.32**
Spain	7.86	9.80	8.76	8.32	8.69	**7.16**
Sweden	6.45	5.49	7.72	8.11	6.94	**5.45**
Switzerland	11.15	9.02	11.52	9.33	10.25	8.86
United Kingdom	11.38	9.75	11.99	14.86	12.00	**9.46**

Table S3. Population weighted average of $PM_{2.5}$ concentrations for all the European countries considered in this work, during the resumption period (May 17 – June 30) over the years 2016-2020. Values in bold indicate that the difference between PM2.5 concentrations in 2020 and the average of 2016-2019 are statistically significant at 1% significance level (with a paired t-test on daily averages).

Country	2016	2017	2018	2019	2016-2019 mean	2020
Austria	7.16	8.59	9.65	9.27	8.67	**6.22**
Belgium	12.46	8.24	13.53	9.04	10.82	**7.50**
Bosnia and Herzegovina	10.67	12.79	12.96	11.84	12.07	**9.70**
Bulgaria	11.43	12.41	12.28	13.77	12.47	**9.55**
Croatia	8.75	10.45	10.47	10.41	10.02	**7.39**
Czech Republic	10.73	9.84	12.75	10.99	11.08	**8.33**
Denmark	9.56	7.76	8.68	7.77	8.45	**6.39**
Estonia	6.80	5.48	5.36	6.25	5.97	6.45
Finland	5.51	4.04	4.60	5.36	4.88	5.32
France	8.69	8.20	9.79	7.92	8.65	**6.22**
Germany	9.63	9.24	10.92	9.25	9.76	**7.13**
Greece	12.24	12.68	12.24	14.69	12.96	**8.91**
Hungary	10.15	10.71	10.73	10.48	10.52	**8.25**
Ireland	6.66	4.74	8.77	5.72	6.47	5.81
Italy	9.66	11.38	10.12	11.29	10.61	**7.47**
Lithuania	11.01	9.47	9.04	8.71	9.56	**7.89**
Luxembourg	7.79	7.03	8.66	6.53	7.50	**5.99**
Malta	10.23	11.19	11.42	11.33	11.04	**8.59**
Netherlands	10.58	8.33	13.16	8.87	10.23	**7.45**
Norway	6.42	5.15	6.31	5.47	5.84	5.62
Poland	12.98	11.08	12.22	11.77	12.01	**9.84**
Portugal	5.61	8.75	7.59	5.07	6.75	6.12
Republic of Macedonia	10.03	12.68	11.41	15.96	12.52	**10.94**
Serbia	10.46	12.61	12.67	12.91	12.16	**10.33**
Slovakia	11.64	10.60	11.43	11.03	11.18	**9.15**
Spain	8.82	10.49	9.73	7.54	9.14	**6.91**
Sweden	6.27	4.98	5.26	6.33	5.71	5.46
Switzerland	5.86	8.40	7.75	7.84	7.46	**5.66**
United Kingdom	8.70	8.01	11.86	7.93	9.13	**7.42**

Table S4. Population weighted average of $PM_{2.5}$ concentrations for all provinces in China, during the lockdown period (February 1 – March 31) over the years 2016-2020. Values in bold indicate that the difference between $PM_{2.5}$ concentrations in 2020 and the average of 2016-2019 are statistically significant at 1% significance level (with a paired t-test on daily averages).

Province	2016	2017	2018	2019	2016-2019 mean	2020
Anhui Province	68.37	71.86	60.37	63.91	66.13	**42.91**
Beijing Municipality	64.24	65.93	68.27	52.48	62.73	47.39
Chongqing Municipality	61.15	48.45	47.26	42.59	49.86	**40.25**
Fujian Province	35.27	33.17	33.29	26.44	32.04	**23.31**
Gansu province	41.48	44.37	44.99	35.33	41.54	**31.49**
Guangdong Province	36.63	37.78	38.98	25.52	34.73	**22.67**
Guangxi Zhuang Autonomous Region	45.84	42.94	49.32	29.47	41.89	**29.36**
Guizhou Province	43.17	34.92	42.01	27.76	36.97	**29.84**
Hainan Province	24.03	21.85	24.43	15.41	21.43	**13.31**
Hebei Province	68.72	79.13	77.10	71.00	73.99	**49.73**
Heilongjiang Province	38.78	38.18	41.79	53.21	42.99	**35.24**
Henan Province	77.69	82.44	76.00	80.77	79.22	**52.73**
Hong Kong Special Administrative Region	29.13	29.17	27.91	19.90	26.53	**19.20**
Hubei Province	69.18	61.20	57.52	53.30	60.30	**38.25**
Hunan Province	58.47	47.92	50.53	39.47	49.10	**33.30**
Inner Mongolia Autonomous Region	36.75	35.20	36.40	33.47	35.46	30.39
Jiangsu Province	68.31	60.76	57.13	58.55	61.19	**37.14**
Jiangxi Province	50.69	47.02	43.62	29.27	42.65	**25.87**
Jilin Province	44.99	50.77	47.05	54.39	49.30	**34.52**
Liaoning Province	49.84	58.93	54.90	56.14	54.95	**40.43**
Ningxia Hui Autonomous Region	50.00	47.98	46.47	38.36	45.70	**34.09**
Qinghai Province	44.74	39.47	40.49	30.78	38.87	**26.34**
Shaanxi Province	60.57	70.01	66.24	62.44	64.81	**48.32**
Shandong Province	75.82	70.32	61.00	73.00	70.03	**47.47**
Shanghai Municipality	53.84	47.80	43.34	46.59	47.89	**28.69**
Shanxi Province	55.25	70.12	69.98	61.23	64.15	**45.01**
Sichuan Province	59.02	50.02	53.69	43.12	51.46	**39.69**
Taiwan Province	34.20	31.41	29.07	24.81	29.87	**23.70**
Tianjin Municipality	65.89	75.42	70.48	66.13	69.48	**50.25**
Tibet Autonomous Region	23.29	18.78	17.52	11.72	17.83	**10.09**
Xinjiang Uygur Autonomous Region	112.18	79.01	74.27	72.82	84.57	72.10
Yunnan Province	37.84	35.19	38.46	29.46	35.24	32.85
Zhejiang Province	52.53	48.31	41.86	35.40	44.52	**24.75**

Table S5. Population weighted average of $PM_{2.5}$ concentrations for all provinces in China, during the resumption period (April 1 – June 30) over the years 2016-2020. Values in bold indicate that the difference between $PM_{2.5}$ concentrations in 2020 and the average of 2016-2019 are statistically significant at 1% significance level (with a paired t-test on daily averages).

Province	2016	2017	2018	2019	2016-2019 mean	2020
Anhui Province	41.61	47.63	41.42	33.33	41.00	**28.47**
Beijing Municipality	53.90	49.78	50.70	37.95	48.08	**31.10**
Chongqing Municipality	37.65	31.42	28.54	25.67	30.82	**24.57**
Fujian Province	25.41	23.64	26.29	22.35	24.42	**18.50**
Gansu province	28.63	30.32	32.98	24.79	29.18	**21.92**
Guangdong Province	25.08	26.08	25.31	18.31	23.70	**17.13**
Guangxi Zhuang Autonomous Region	27.83	28.21	27.22	22.82	26.52	**21.97**
Guizhou Province	26.15	24.07	25.10	19.99	23.83	**19.86**
Hainan Province	14.57	13.69	13.55	12.12	13.48	**11.26**
Hebei Province	50.54	52.41	45.51	37.17	46.41	**31.51**
Heilongjiang Province	23.30	26.99	25.64	18.82	23.69	24.59
Henan Province	48.35	49.58	42.75	37.00	44.42	**32.24**
Hong Kong Special Administrative Region	17.56	19.08	17.70	14.25	17.15	**12.94**
Hubei Province	36.74	38.08	34.57	30.80	35.05	**26.82**
Hunan Province	33.00	30.17	29.69	26.66	29.88	**25.29**
Inner Mongolia Autonomous Region	28.22	27.93	27.79	23.26	26.80	**20.92**
Jiangsu Province	43.15	43.00	42.89	33.39	40.61	**31.71**
Jiangxi Province	30.25	33.73	29.21	25.20	29.60	**23.17**
Jilin Province	27.45	30.30	28.40	22.30	27.11	32.07
Liaoning Province	35.32	34.65	32.72	29.07	32.94	29.62
Ningxia Hui Autonomous Region	33.16	36.12	37.59	28.51	33.84	**24.29**
Qinghai Province	31.64	25.51	32.79	23.56	28.37	**20.66**
Shaanxi Province	35.66	36.83	36.12	32.23	35.21	**26.78**
Shandong Province	52.94	49.30	40.49	36.94	44.92	**33.82**
Shanghai Municipality	45.04	36.93	38.30	30.55	37.71	**31.04**
Shanxi Province	40.06	43.07	43.38	34.26	40.19	**30.46**
Sichuan Province	36.62	32.26	31.17	26.32	31.59	**25.92**
Taiwan Province	24.07	22.18	22.66	19.72	22.16	**16.87**
Tianjin Municipality	54.39	54.83	47.49	39.96	49.17	**35.13**
Tibet Autonomous Region	21.12	15.95	16.68	11.47	16.30	**9.88**
Xinjiang Uygur Autonomous Region	50.56	39.50	54.12	31.20	43.84	39.16
Yunnan Province	24.17	24.58	24.29	24.92	24.49	**20.75**
Zhejiang Province	35.74	33.52	32.72	26.87	32.21	**24.41**

Table S6. P-values of paired t-test to compare daily population weighted $PM_{2.5}$ mean in different years, during the lockdown period (February 21 – May 17) in Europe.

	2016	2017	2018	2019	2020
2016	-	0.28	0.00089	0.71	0.00063
2017	-	-	0.00018	0.30	0.0040
2018	-	-	-	0.0020	<0.0001
2019	-	-	-	-	0.00082
2020	-	-	-	-	-

Table S7. P-values of paired t-test to compare daily population weighted $PM_{2.5}$ mean in different years, during the lockdown period (February 1 – March 31) in China. Differences between pairwise years 2016-2019 are not statistically significant at a 5% significance level (except for the pair 2016-2019, which is weakly significant), whereas a strongly significant difference is observed between 2020 and all previous years.

	2016	2017	2018	2019	2020
2016	-	0.42	0.090	0.043	<0.0001
2017	-	-	0.22	0.14	<0.0001
2018	-	-	-	0.84	<0.0001
2019	-	-	-	-	<0.0001
2020	-	-	-	-	-

Additional references

1 EEA. *Air pollution goes down as Europe takes hard measures to combat coronavirus*, 2020).

2 Tobías, A. *et al.* Changes in air quality during the lockdown in Barcelona (Spain) one month into the SARS-CoV-2 epidemic. *Science of The Total Environment*, 138540 (2020).

3 Dutheil, F., Baker, J. S. & Navel, V. COVID-19 as a factor influencing air pollution? *Environmental Pollution* **263**, 114466, doi:https://doi.org/10.1016/j.envpol.2020.114466 (2020).

4 Wang, X., Dickinson, R. E., Su, L., Zhou, C. & Wang, K. PM2.5 Pollution in China and How It Has Been Exacerbated by Terrain and Meteorological Conditions. *Bulletin of the American Meteorological Society* **99**, 105-119, doi:10.1175/bams-d-16-0301.1 (2018).

5 Chin, M. Dirtier air from a weaker monsoon. *Nature Geoscience* **5**, 449-450, doi:10.1038/ngeo1513 (2012).

6 Cressie, N. *Statistics for Spatial Data*. (Wiley, 1993).

7 Yang, Y. *et al.* Uncertainty assessment of $PM_{2.5}$ contamination mapping using spatiotemporal sequential indicator simulations and multi-temporal monitoring data. *Scientific reports* **6**, 1-13 (2016).

8 Giani, P., Anav, A., De Marco, A., Zhaozhong, F. & Crippa, P. Exploring sources of uncertainty in premature mortality estimates from fine particulate matter: the case of China. *Environmental Research Letters* (2020).

9 Lowen, A. C. & Steel, J. Roles of Humidity and Temperature in Shaping Influenza Seasonality. *Journal of Virology* **88**, 7692-7695, doi:10.1128/jvi.03544-13 (2014).

10 Dushoff, J., Plotkin, J. B., Levin, S. A. & Earn, D. J. D. Dynamical resonance can account for seasonality of influenza epidemics. *Proceedings of the National Academy of Sciences of the United States of America* **101**, 16915-16916, doi:10.1073/pnas.0407293101 (2004).

11 Luo, W. *et al.* The role of absolute humidity on transmission rates of the COVID-19 outbreak. *medRxiv*, 2020.2002.2012.20022467, doi:10.1101/2020.02.12.20022467 (2020).

12 Hong, S. Y. & J. Lim, J. O. *The WRF single-moment 6-class microphysics scheme (WSM6)*. Vol. 42 (2006).

13 Tiedtke, M. A Comprehensive Mass Flux Scheme for Cumulus Parameterization in Large-Scale Models. *Monthly Weather Review* **117**, 1779-1800, doi:10.1175/1520-0493(1989)117<1779:acmfsf>2.0.co;2 (1989).

14 Iacono, M. J. *et al.* Radiative forcing by long-lived greenhouse gases: Calculations with the AER radiative transfer models. *Journal of Geophysical Research: Atmospheres* **113**, doi:10.1029/2008jd009944 (2008).

15 Chen, F. & Dudhia, J. Coupling an Advanced Land Surface–Hydrology Model with the Penn State–NCAR MM5 Modeling System. Part I: Model Implementation and Sensitivity. *Monthly Weather Review* **129**, 569-585, doi:10.1175/1520-0493(2001)129<0569:caalsh>2.0.co;2 (2001).

16 Hong, S. Y., Noh, Y. & Dudhia, J. A new vertical diffusion package with an explicit treatment of entrainment processes. *Monthly Weather Review* **134**, 2318-2341, doi:10.1175/mwr3199.1 (2006).

17 Emmons, L. K. *et al.* Description and evaluation of the Model for Ozone and Related chemical Tracers, version 4 (MOZART-4). *Geosci. Model Dev.* **3**, 43-67, doi:10.5194/gmd-3-43-2010 (2010).

18 Chin, M., Rood, R. B., Lin, S.-J., Müller, J.-F. & Thompson, A. M. Atmospheric sulfur cycle simulated in the global model GOCART: Model description and global properties. *Journal of Geophysical Research: Atmospheres* **105**, 24671-24687, doi:10.1029/2000jd900384 (2000).

19 Madronich, S. Photodissociation in the atmosphere: 1. Actinic flux and the effects of ground reflections and clouds. *Journal of Geophysical Research: Atmospheres* **92**, 9740-9752 (1987).

20 Guenther, A. B. *et al.* The Model of Emissions of Gases and Aerosols from Nature version 2.1 (MEGAN2.1): an extended and updated framework for modeling biogenic emissions. *Geosci. Model Dev.* **5**, 1471-1492, doi:10.5194/gmd-5-1471-2012 (2012).

21 Janssens-Maenhout, G. *et al.* HTAP_v2.2: a mosaic of regional and global emission grid maps for 2008 and 2010 to study hemispheric transport of air pollution. *Atmos. Chem. Phys.* **15**, 11411-11432, doi:10.5194/acp-15-11411-2015 (2015).

22 Wiedinmyer, C. *et al.* The Fire INventory from NCAR (FINN): a high resolution global model to estimate the emissions from open burning. *Geosci. Model Dev.* **4**, 625-641, doi:10.5194/gmd-4-625-2011 (2011).

23 Ginoux, P. *et al.* Sources and distributions of dust aerosols simulated with the GOCART model. *Journal of Geophysical Research: Atmospheres* **106**, 20255-20273, doi:10.1029/2000jd000053 (2001).

24 Gong, S. L. A parameterization of sea-salt aerosol source function for sub- and super-micron particles. *Global Biogeochemical Cycles* **17**, doi:10.1029/2003gb002079 (2003).

25 C3S. (ed Copernicus Climate Change Service) (https://cds.climate.copernicus.eu/cdsapp#!/home, Copernicus Climate Change Service Climate Data Store (CDS), 2017).

26 Bai, K., K. Li, N.-B. Chang, and W. Gao (2019), Advancing the prediction accuracy of satellite-based PM2. 5 concentration mapping: A perspective of data mining through in situ PM2. 5 measurements, Environmental Pollution, 254, 113047

27 Xue, T., Y. Zheng, D. Tong, B. Zheng, X. Li, T. Zhu, and Q. Zhang (2019), Spatiotemporal continuous estimates of PM2. 5 concentrations in China, 2000–2016: A machine learning method with inputs from satellites, chemical transport model, and ground observations, Environment international, 123, 345-357.